Magnetic Resonance Brain Image Classification Based on Weighted-Type Fractional Fourier Transform and Nonparallel Support Vector Machine

Yu-Dong Zhang,[1,2] Shufang Chen,[3] Shui-Hua Wang,[1,2] Jian-Fei Yang,[2] Preetha Phillips[4]

[1] School of Computer Science and Technology, Nanjing Normal University, Nanjing, Jiangsu, 210023, China

[2] Jiangsu Key Laboratory of 3D Printing Equipment and Manufacturing, Nanjing, Jiangsu, 210042, China

[3] School of Communication and Information Engineering, University of Electronic Science and Technology of China, Chengdu, Sichuan, 611731, China

[4] School of Natural Sciences and Mathematics, Shepherd University, Shepherdstown, WV 25443

Received 1 August 2015; revised 6 October 2015; accepted 26 October 2015

ABSTRACT: To classify brain images into pathological or healthy is a key pre-clinical state for patients. Manual classification is tiresome, expensive, time-consuming, and irreproducible. In this study, we aimed to present an automatic computer-aided system for brain-image classification. We used 90 T2-weighted images obtained by magnetic resonance images. First, we used weighted-type fractional Fourier transform (WFRFT) to extract spectrums from each magnetic resonance image. Second, we used principal component analysis (PCA) to reduce spectrum features to only 26. Third, those reduced spectral features of different samples were combined and were fed into support vector machine (SVM) and its two variants: generalized eigenvalue proximal SVM and twin SVM. A 5 × 5-fold cross-validation results showed that this proposed "WFRFT + PCA + generalized eigenvalue proximal SVM" yielded sensitivity of 99.53%, specificity of 92.00%, precision of 99.53%, and accuracy of 99.11%, which are comparable with the proposed "WFRFT + PCA + twin SVM" and better than the proposed "WFRFT + PCA + SVM." Besides, all three proposed methods were superior to eight state-of-the-art algorithms. Thus, WFRFT is effective, and the proposed methods can be used in practical. Int J Imaging Syst Technol, 25, 317–327, 2015; Published online in Wiley Online Library (wileyonlinelibrary.com). DOI: 10.1002/ima.22144

Key words: magnetic resonance imaging; fractional Fourier transform (FRFT); pathological brain detection; weighted-type FRFT; support vector machine (SVM); nonparallel SVM; machine learning

1. BACKGROUND

Magnetic resonance imaging (MRI) offers higher resolution than other imaging techniques and is becoming the most popular imaging modality in the hospital (Yu et al., 2015). However, to make a diagnosis usually needs human eyes manually. Existing manual methods are tedious, time-consuming, or costly, because of the enormous volume of magnetic resonance (MR) imaging data. The main disadvantage of manual methods is its irreducibility, which leads to the necessity to propose a computer-aided diagnosis platform (Thorsen et al., 2013) for MR images (Goh et al., 2014; Zhang et al., 2015c).

In this study, we focus on the brain because it is the most important part of the body. Recently, a variety of systems were provided for classification of brain MR images. Those methods can be divided into two types according to the data dimension. One type is for 3D image, but it needs to scan the whole brain. The other type is based on a single-slice that contains the disease-related areas, which is cheap and commonly used in Chinese hospitals. Chaplot et al. (2006) used an advanced signal-processing technique named "discrete wavelet transform" (DWT) to obtain the approximation coefficients.

Correspondence to: S. H. Wang; e-mail: wangshuihua@njnu.edu.cn

Grant sponsor: NSFC, Grant numbers: 61273243; 51407095

Grant sponsor: Natural Science Foundation of Jiangsu Province, Grant numbers: BK20150982; BK20150983

Grant sponsor: Priority Academic Program Development of Jiangsu Higher Education Institutions (PAPD), Jiangsu Key Laboratory of 3D Printing Equipment and Manufacturing, Grant number: BM2013006

Grant sponsor: Key Supporting Science and Technology Program (Industry) of Jiangsu Province, Grant number: BE2013012-2 and BE2014009-3

Grant sponsor: Program of Natural Science Research of Jiangsu Higher Education Institutions, Grant numbers: 13KJB460011; 14KJB520021

Grant sponsor: Special Funds for Scientific and Technological Achievement Transformation Project in Jiangsu Province, Grant number: BA2013058

Grant sponsor: Nanjing Normal University Research Foundation for Talented Scholars, Grant number: 2013119XGQ0061 and 2014119XGQ0080

Grant sponsor: Education Reform Project in NJNU, Grant number: 18122000090615

They utilized both support vector machine (SVM) and self-organizing map for classification. Georgiadis et al. (2008) designed and evaluated a software system for discriminating between metastatic and primary brain tumors on MRI. They proposed a modified probabilistic neural network (PNN), incorporating a nonlinear least squares features transformation into the PNN classifier. Wang and Wu (2010) used forward neural network (FNN) to classify a particular MR brain image as pathological or healthy. The parameters of FNN were optimized via a variant of particle swarm optimization (PSO), i.e., adaptive chaotic PSO. Results over 160 images showed that the classification accuracy was 98.75%. El-Dahshan et al. (2010) used the coefficients of a three-level DWT, and decreased the number of features by principal component analysis (PCA). They finally used K-nearest neighbors and feed-forward back-propagation artificial neural network (ANN) for brain classification. Wu and Wang (2011) proposed to use DWT for feature extraction, PCA for feature reduction, and FNN with a variant of artificial bee colony (ABC), viz., scaled chaotic ABC (SCABC), for classification. After consecutive research, Dong et al. (2011) further discussed the possibility to take the place of SCABC with a novel scaled conjugate gradient method. Zhang and Wu (2012) suggested to use kernel SVM (KSVM), and offered three new kernels: homogeneous polynomial, Gaussian radial basis, and inhomogeneous polynomial. Ramasamy and Anandhakumar (2011) then presented a fast-Fourier-transform based expectation–maximization Gaussian mixture model for brain classification of MR images. Saritha et al. (2013) were the first to use wavelet-entropy (WE) in MR brain classification. They harnessed spider-web plots to decrease the WE features. They used the PNN for classification. After full investigation on Saritha et al.'s work, Zhang et al. (2015a) pointed out that removing spider-web plot yielded the same classification performance. Padma and Sukanesh (2014) used combined wavelet statistical texture features, to segment and classify Alzheimer's disease (AD) benign and malignant tumor slices. Das et al. (2013) were the first to combine Ripplet transform and PCA in MR brain classification. They used a least square SVM as the classifier. Their 5×5 cross-validation (CV) test showed high classification accuracies. Zhang et al. (2013) suggested to use PSO to train the KSVM. El-Dahshan et al. (2014) used the feedback pulse-coupled neural network for image segmentation, the DWT for features extraction, the PCA for reducing the dimensionality of the wavelet coefficients, and the FBPNN to classify inputs into normal or abnormal. Wang et al. (2014) presented a diagnosis method to distinguish AD and mild cognitive impairment from normal controls, based on structural MR images by the combination of KSVM and decision tree. A fivefold CV showed that their method yielded an accuracy of 80% for these three classes. Zhou et al. (2015) again used WE as the feature space, and then they used the traditional Naive Bayes classifier classification method. Their results over more than 60 images showed that the sensitivity was 94.50%, the specificity 91.70%, and the overall accuracy 92.60%. Zhang et al. (2015e) utilized an advanced variant of DWT, i.e., the discrete wavelet packet transform, and used Tsallis entropy to replace traditional Shannon entropy with the aim of obtaining features from discrete wavelet packet transform coefficients. Then, they suggested to harness a generalized eigenvalue proximal SVM (GEPSVM). Afterward, RBF kernel was suggested to augment the classification performance. Damodharan and Raghavan (2015) combined tissue segmentation and neural network for brain tumor detection. Yang et al. (2015) selected wavelet-energy as the feature and introduced biogeography-based optimization (BBO) to train the SVM. Their method reached 97.78% accuracy on 90 T2-weighted MR brain images. Guang-Shuai et al. (2015) used wavelet-energy and SVM. Their results obtained only 82.69% accuracy. Wang et al. (2015a) proposed a combination of genetic algorithm (GA) and KSVM to solve this problem. Nazir et al. (2015) offered an approach to use filters for removing noises and extracted the "color moments" as main features. Finally, they achieved an overall accuracy of 91.8%. Zhang et al. (2015d) suggested to use an eigenbrain method to detect subjects and brain regions related to AD. The accuracy achieved $92.36\% \pm 0.94\%$. Harikumar and Kumar (2015) analyzed the performance of ANN in classification of medical images using wavelets as features. The classification result of 96% was achieved using the RBF and db4 wavelet. Wang et al. (2015c) used stationary wavelet transform to replace DWT, and then they proposed a hybridization of ABC and PSO algorithm to train the classifier. Zhang et al. (2015f) proposed a novel hybridization of BBO and PSO methods, and named it as HBP, for MR brain classification. Munteanu et al. (2015) used proton MR spectroscopy data, with the aim of detecting mild cognitive impairment and AD. They used a single-layer perceptron with only two spectroscopic voxel volumes obtained in the left hippocampus, with an AUROC value of 0.866. Zhang et al. (2015b) suggested to use stationary wavelet transform and to use generalized GEPSVM for classification. Their algorithm achieved 99.41% accuracy over a 255-image dataset. Savio and Grana (2015) utilized local activity features, such as regional homogeneity, to develop a computer-aided diagnosis of schizophrenia on resting-state function MRI. Zhang et al. (2015h) combined wavelet-entropy with Hu moment invariants. The feature number is in total 14. They also used GEPSVM as the classifier. Wibmer et al. (2015) investigated Haralick texture analysis to detect cancer in prostate MRI. Zhang and Wang (2015) used 2D displacement field to detect AD. Their method achieved an accuracy of $92.75\% \pm 1.77\%$, sensitivity of $90.56\% \pm 1.15\%$, specificity of $93.37\% \pm 2.05\%$, and precision of $79.61\% \pm 2.21\%$.

After analyzing the aforementioned methods, we found that most of them transformed the image to wavelet-domain, which has a problem of how to determine the optimal decomposition level and optimal wavelet (Fang et al., 2015). Therefore, we proposed to use fractional Fourier transform (FRFT) that can transform images from the spatial domain to the "unified time-frequency domain." Reports have clearly shown that the unified time-frequency domain is more suitable for classification than the traditional frequency domain and wavelet domain (Bhaduri et al., 2010; Ajmera and Holambe, 2013; Seok and Bae, 2014).

SVMs are gaining popularity in pattern recognition. Nevertheless, the hyperplanes of SVM should be parallel. In the recent years, scholars have suggested to discard the parallelism of hyperplanes in SVM (Mehrkanoon et al., 2014). Hence, we introduced two variants of SVM. They are GEPSVM and twin SVM (TSVM). We compared them with original SVM in the experiments.

The structure of the article is organized as follows: Section contains the materials and methods. Section contains the experiments, results, and discussions. Section contains the conclusion and future research.

2. MATERIALS AND METHODS

A. Dataset. The dataset *brain* contains 90 T2-weighted MR brain images, which are obtained along the axial plane. The image sizes are all 256×256 in pixel. The dataset can be downloaded from the webpage of Medical School of Harvard University (URL: www.med.harvard.edu/aanlib/home.html). Pathological brain images within the dataset cover 17 different illnesses, each disease from

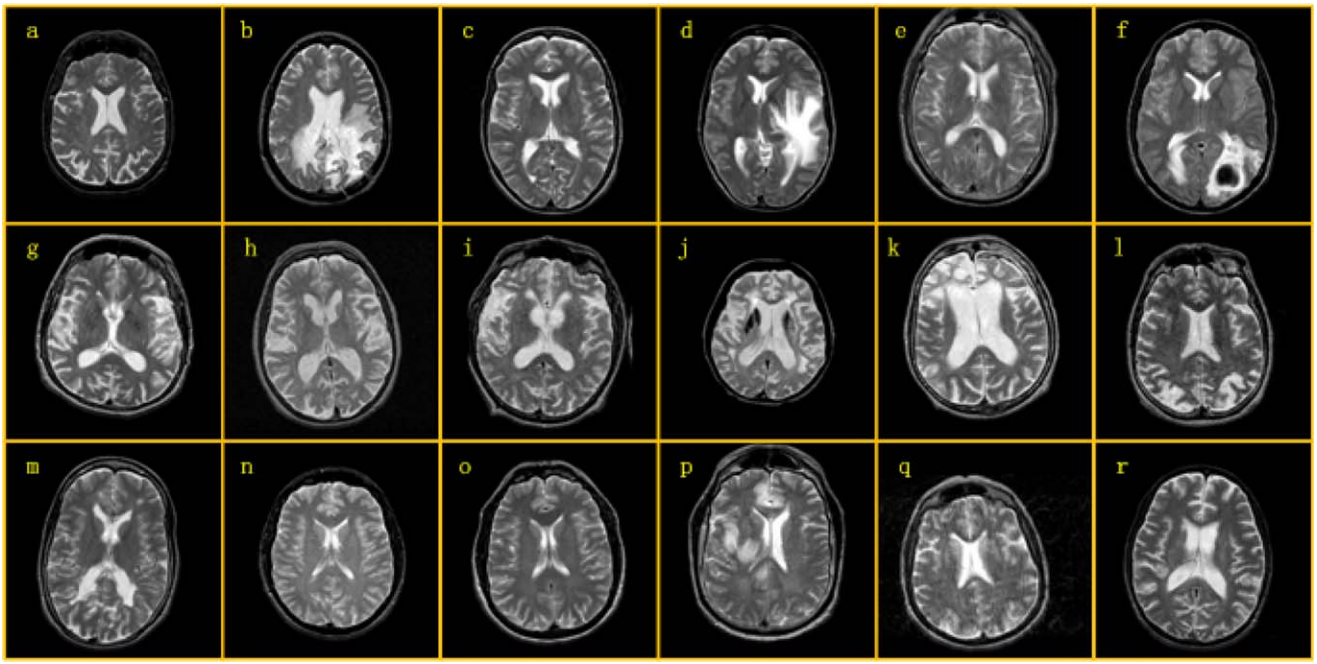

Figure 1. Brain MR images: (a) A healthy brain; (b) Glioma; (c) Metastatic adenocarcinoma; (d) Metastatic bronchogenic carcinoma; (e) Meningioma; (f) Sarcoma; (g) Alzheimer's disease; (h) Huntington's disease; (i) Motor neuron disease; (j) Cerebral calcinosis; (k) Pick's disease; (l) Alzheimer's disease plus visual agnosia; (m) Multiple sclerosis; (n) AIDS dementia; (o) Lyme encephalopathy; (p) Herpes encephalitis; (q) Creutzfeldt-Jakob disease; and (r) Cerebral toxoplasmosis. [Color figure can be viewed in the online issue, which is available at wileyonlinelibrary.com.]

different subjects. Most patients of brain diseases are disobedient, so it is very difficult to obtain their brain images. The samples of each disease are illustrated in Figure 1.

Note that we performed an initial study here. We treated both brain tumors and neurodegenerative diseases as pathological brains. Hence, our task is a binary classification problem, i.e., to detect pathological brain from healthy brains. Besides, we invite physicians to re-check the disease type of each MR brain image.

We did not use traditional statistical methods such as Monte Carlo; instead, the most advanced CV method was used. Five images were randomly selected for each type of disease. Because there are one type of healthy brain and 17 types of pathological brain in the dataset, $5 \times (1 + 17) = 90$ images were selected to construct the *brain* dataset, consisting of five healthy and 85 pathological brain images in total. In this study, a 5×5-fold CV was implemented, with the aim of reducing randomness. The confusion matrices of five runs were combined to form the final confusion matrix, with the ideal results of 425 pathological instances and 25 healthy instances perfectly recognized.

Note that the leave-one-out CV will run the same times as the number of observations in the dataset. We did not use the leave-one-out CV so as to save computation time.

B. Fractional Fourier Transform. The Fourier transform (FT) decomposes a time signal into the frequencies; hence, the FT is also called frequency domain representation of the original signal (Ajmera and Holambe, 2013). It served an important role in various academic and industrial fields and is applied successfully in many scientific and technological domains.

However, FT was reported to have some shortcomings, as it cannot analyze nonstationary signals. Therefore, novel variants of FT were proposed in the last decade. The most successful among them is FRFT, which can transform a signal/image to any intermediate domain between time and frequency, viz., the unified time-frequency transform.

For any real α, the α-angle FRFT of a function $x(t)$ was denoted by X_α and defined with the form of

$$X_\alpha(u) = F_\alpha[x] = \int_{-\infty}^{\infty} x(t) K_\alpha(t,u)\, dt \tag{1}$$

where, u is the frequency, t the time, and K the transform kernel with the form of

$$K_\alpha(t,u) = \sqrt{1 - j\cot\alpha}\, \exp\left(j\pi(t^2\cot\alpha - 2ut\csc\alpha + u^2\cot\alpha)\right) \tag{2}$$

where, j is the imaginary unit. The cot and csc functions will diverge if α is a multiple of π. This can be coped with taking the limit, which leads to following a clearer expression

$$K_\alpha(t,u) = \begin{cases} \sqrt{1 - j\cot\alpha}\, \exp(j\pi(t^2\cot\alpha - 2ut\csc\alpha + u^2\cot\alpha)) & \alpha \neq m\pi \\ \delta(t-u) & \alpha = 2m\pi \\ \delta(t+u) & \alpha = (2m+1)\pi \end{cases} \tag{3}$$

where, m is the arbitrary integer and δ the Diract delta function. In some references, scholars used angular frequency ω, and the FRFT can be defined with following form

$$X_\alpha(\omega) = F_\alpha[x] = \int_{-\infty}^{\infty} x(t) K_\alpha(t,\omega)\, dt \tag{4}$$

where,

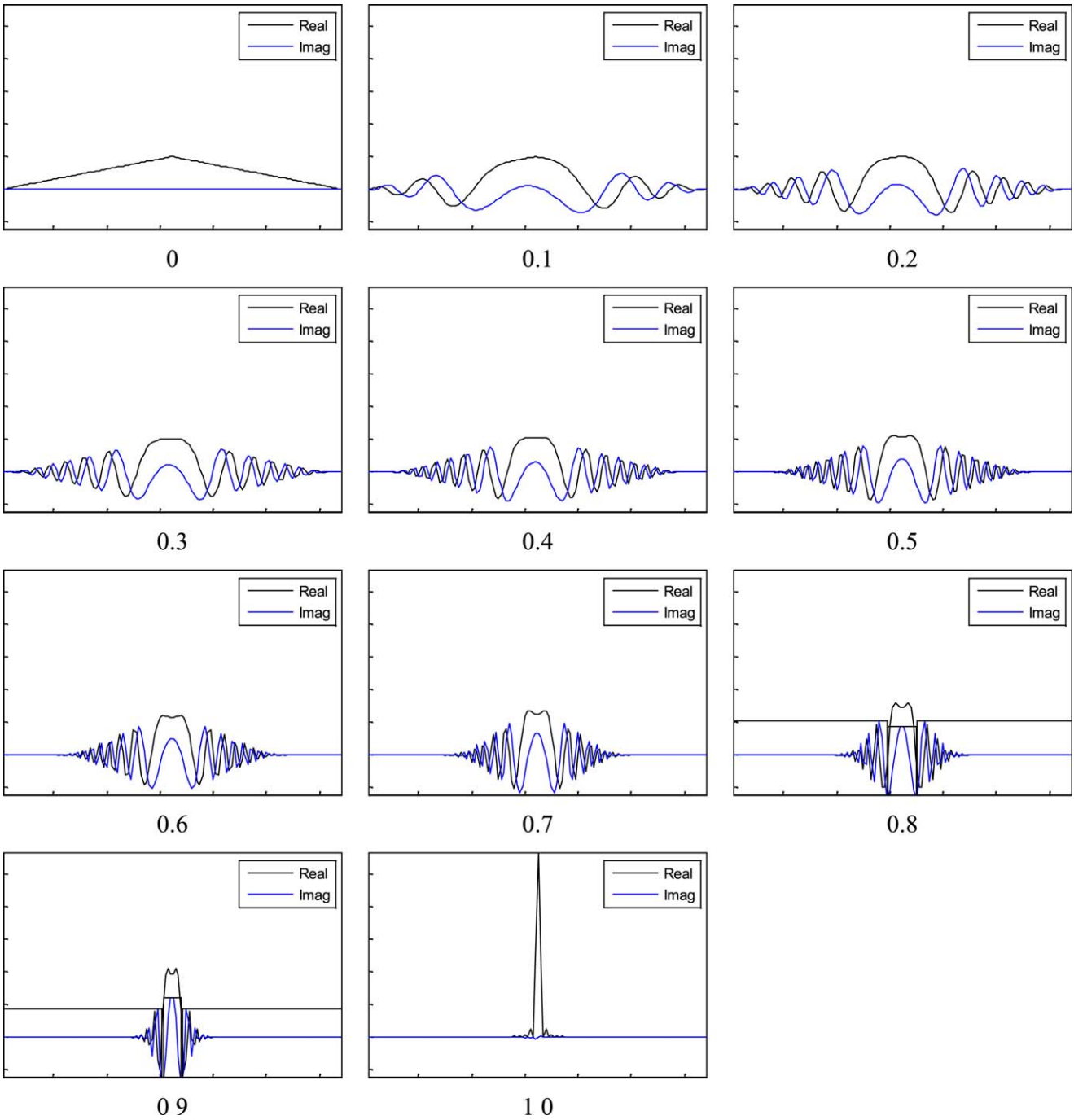

Figure 2. Illustration of FRFT (α changes from 0 to 1). [Color figure can be viewed in the online issue, which is available at wileyonlinelibrary.com.]

$$K_\alpha(t,\omega)=\sqrt{\frac{1-j\cot\alpha}{2\pi}}\exp\left(j\left(\frac{t^2+\omega^2}{2}\right)\cot\alpha-t\omega\csc\alpha\right). \quad (5)$$

In this study, 2D-FRFT was performed by first applying 1D-FRFT to columns and then to rows, or vice versa, because of the linearity of FRFT (Cagatay and Datcu, 2015). Additional to it, there are two angles, α_x and α_y, for 2D-FRFT. When $\alpha_x=\alpha_y=0$, the FRFT becomes an identity operator. When $\alpha_x=\alpha_y=1$, the FRFT degrades to conventional FT.

C. Unified Time-Frequency Domain. To illustrate the meaning of the angle α and the unified time-frequency domain, an example for 1D signal was carried out. Here, a triangular function tri(t) in time domain (Damarla and Kundu, 2015) is used.

$$\mathrm{tri}(t)=\max(1-|t|,0). \quad (6)$$

For a standard FT, the frequency spectrum turns a 2-power of sinc function, viz., $\mathrm{sinc}^2(u)$. Remember that sinc function is defined as

$$\mathrm{sinc}(x)=\frac{\sin(x)}{x}. \tag{7}$$

Furthermore, the results of FRFT with angles from 0 to 1 are listed in Figure 2. The real and imaginary parts were plotted in black and blue lines, respectively. It was clear that FRFT output in the domain between time and frequency, i.e., a unified time-frequency domain.

In this study, we set both α_x and α_y vary from 0.6 to 1 with equal increase of 0.1. We did not consider the range from 0 to 0.5 because FRFT with angles close to 0 will yield an identity operation (see Fig. 2).

D. Weighted-Type FRFT. FRFT is a concept, and weighted-type FRFT (WFRFT) is one of its simplest calculation methods. WFRFT replaces the continuous variables u and t in FRFT, by their discrete versions k and n, respectively. It is defined by the following form (Shih, 1995; Santhanam and McClellan, 1996):

$$F_\alpha=\sum_{i=0}^{3} a_i(\alpha)F_i \tag{8}$$

$$a_i(\alpha)=\frac{1}{4}\sum_{k=1}^{4}\exp\left[j\left(\alpha-i\frac{\pi}{2}\right)k\right]. \tag{9}$$

Then, this kind of FRFT of signal x can be written in the form of

$$X_\alpha = F_\alpha x. \tag{10}$$

It is clear from Eq. (8) that this definition is the linear weighted combination of (1) discrete Fourier transform (DFT) matrix, (2) time inverse matrix, (3) identity matrix, and (4) inverse DFT matrix. It obeys the rotation principle of fractional FT, and it can be implemented by fast algorithms. However, it does not offer transform results similar to those of fractional FT (Ozaktas et al., 1996). By using WFRFT, we generated 25 spectrums from original image, i.e., $256 \times 256 \times 25 = 1{,}638{,}400$ new features were generated.

E. Principal Component Analysis. Excessive features may complicate the subsequent classifier and increase computational resources. The PCA effectively decreases the data dimensionality; hence, it reduces the computation complexity of following data analysis.

PCA is a standard statistical tool, which used a preset orthogonal transformation to convert a set of observations (containing possibly correlated variables) into a set of new observations of linearly uncorrelated variables, which are dubbed as principal components (PCs). Detailed procedures of implementing PCA can be found in literatures (Kuroda et al., 2011; Wu and Zhang, 2012).

F. Support Vector Machine. ANN (Wang et al., 2015d) and SVM are the two most popular methods in classification. Now scholars have proven SVM is better than ANN because of its excellent generalization ability, i.e., SVM will perform better than ANN for new instances (Rodriguez-Galiano et al., 2015).

Suppose there is a p-dimensional N-point training dataset. The dataset can be formulated as

$$\{(x_i, y_i)|x_i \in R^p, y_i \in \{-1, +1\}\},\ \ i=1, 2, 3, \ldots, N. \tag{11}$$

Here, x denotes a p-dimensional training point, y_i is either -1 or $+1$, denoting that the sample can be in Class 1 or Class 2. The aim is to generate a $(p-1)$-dimensional hyperplane as

$$\mathbf{w}x-\mathbf{b}=0. \tag{12}$$

Here, $\mathbf{w}$ and $\mathbf{b}$ denote the weights and biases, respectively. Their values are optimized with the criterion to maximize the distance between the two hyperplanes that are parallel, while still separating the data.

$$\begin{aligned}&\min_{b,\mathbf{w}} \|\mathbf{w}\|^2/2\\ &\text{s.t. } y_i(\mathbf{w}x_i-\mathbf{b}) \geq 1,\ i=1, 2, 3, \ldots, N.\end{aligned} \tag{13}$$

G. Generalized Eigenvalue Proximal SVM. In original SVM, two parallel planes are generated such that each plane is closest to one of the two datasets, and the two planes are as far apart as possible (Wang et al., 2014). Mangasarian and Wild (2006) proposed the GEPSVM. It drops the parallelism condition on the two hyperplanes (remember the parallelism is necessary in original SVM) and requires each hyperplane be as close as possible to one of the datasets and as far as possible from the other dataset. Latest literatures showed that GEPSVM achieved superior classification performance to canonical SVMs (Khemchandani et al., 2011; Shao et al., 2013).

Suppose samples are from either Class 1 (denoted by symbol X_1) or Class 2 (denoted by symbol X_2). The GEPSVM finds the two optimal nonparallel planes with the form of

$$\mathbf{w}_1^T x-\mathbf{b}_1=0 \text{ and } \mathbf{w}_2^T x-\mathbf{b}_2=0. \tag{14}$$

To obtain the first plane, we deduce from Eq. (14) and get the following solution

$$(\mathbf{w}_1, \mathbf{b}_1)=\underset{(\mathbf{w},b)\neq 0}{\operatorname{argmin}} \frac{\|\mathbf{w}^T X_1-o^T\mathbf{b}\|^2/\|z\|^2}{\|\mathbf{w}^T X_2-o^T\mathbf{b}\|^2/\|z\|^2} \tag{15}$$

$$z \leftarrow \begin{bmatrix}\mathbf{w}\\ \mathbf{b}\end{bmatrix} \tag{16}$$

where, o is a vector of ones of appropriate dimensions. Simplifying Eq. (15) gives

$$\min_{(\mathbf{w},b)\neq 0} \frac{\|\mathbf{w}^T X_1-o^T b\|^2}{\|\mathbf{w}^T X_2-o^T b\|^2} \tag{17}$$

We include the Tikhonov regularization term to decrease the norm of the variable z that corresponds to the first hyperplane in Eq. (14).

$$\min_{(\mathbf{w},b)\neq 0} \frac{\|\mathbf{w}^T X_1-o^T b\|^2+t\|z\|^2}{\|\mathbf{w}^T X_2-o^T b\|^2} \tag{18}$$

where, t is a positive (or zero) Tikhonov factor. Equation (18) turns to the "Rayleigh quotient" in the following form of

$$z_1=\arg\min_{z\neq 0} \frac{z^T P z}{z^T Q z} \tag{19}$$

where P and Q are symmetric matrices in $\mathbb{R}^{(p+1)\times(p+1)}$ as

$$P \overset{\text{def}}{=} [X_1 \quad -o]^T[X_1 \quad -o]+tI \tag{20}$$

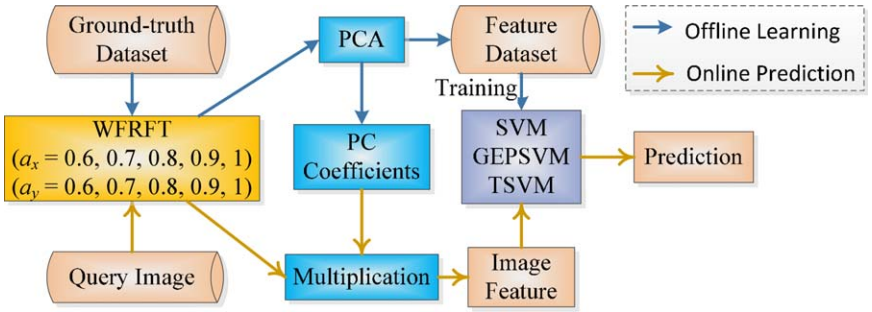

Figure 3. Diagram of the proposed method. [Color figure can be viewed in the online issue, which is available at wileyonlinelibrary.com.]

$$Q \overset{\text{def}}{=} [X_2 \quad -o]^T [X_2 \quad -o] \tag{21}$$

Using the stationarity and boundedness properties of Rayleigh quotient, solution of Eq. (19) is deduced by solving a generalized eigenvalue problem as

$$Pz = \lambda Qz, z \neq 0. \tag{22}$$

Here, the global minimum of Eq. (19) is obtained at an eigenvector z_1 corresponding to the smallest eigenvalue $\lambda_{\min}$ of Eq. (22). Therefore, $\mathbf{w}_1$ and $\mathbf{b}_1$ can be obtained through Eq. (16) and used to determine the plane in Eq. (14). Afterward, a similar optimization problem is generated that is analogous to Eq. (17) by exchanging the symbols of X_1 and X_2. The eigenvector z_2* corresponding to the smallest eigenvalue of the second generalized eigenvalue problem will obtain the second hyperplane approximate to samples of Class 2.

H. Twin SVM. Jayadeva et al. (2007) proposed a novel TSVM. The TSVM is similar to GEPSVM in the way that both obtain nonparallel hyperplanes. The difference lies in that GEPSVM and TSVM are formulated entirely different. Each of the two quadratic programming (QP) problems in TSVM pair is formulated as a typical SVM. Note that QP is a particular optimization problem in mathematics. It optimizes a quadratic function of several variables subject to linear constraints. Many mature approaches have been developed to solve QP problems (Punnen et al., 2015), such as interior point, conjugate gradient, active set, augmented Lagrangian, and simplex algorithms.

Reports have shown that TSVM is better than both SVM and GEPSVM (Nasiri et al., 2014; Shao et al., 2014; Xu et al., 2014). Mathematically, the TSVM is constructed by solving the two QP problems

$$\begin{aligned} &\min_{\mathbf{w}_1, b_1, q} \frac{1}{2}(X_1\mathbf{w}_1 + o_1 b_1)^T (X_1\mathbf{w}_1 + o_1 b_1) + c_1 o_2^T q \\ &\text{s.t.} -(X_2\mathbf{w}_1 + o_2 b_1) + q \geq o_2, q \geq 0 \end{aligned} \tag{23}$$

$$\begin{aligned} &\min_{\mathbf{w}_2, b_2, q} \frac{1}{2}(X_2\mathbf{w}_2 + o_2 b_2)^T (X_2\mathbf{w}_2 + o_2 b_2) + c_2 o_1^T q \\ &\text{s.t.} -(X_1\mathbf{w}_2 + o_1 b_2) + q \geq o_1, q \geq 0. \end{aligned} \tag{24}$$

Here, c_i ($i = 1,2$) are positive parameters, and o_i ($i = 1,2$) is the same as in Eq. (15). By this means, the TSVM constructed two hyperplanes. The first term in Eqs. (23) and (24) is the sum of squared distances from the hyperplane to one class. The second term is the sum of error variables. Therefore, minimizing Eqs. (23) and (24) will keep the hyperplanes close to points of each class and minimize the misclassification rate. Finally, the constraint requires the hyperplane to be at a distance of more than one from points of one class to points of the other class. Another advantage of TSVM is that its convergence rate is four times faster than that of conventional SVM (Jayadeva et al., 2007).

I. Implementation. The aim of this study was to develop an automatic MR brain-image detection system with high accuracy. The proposed system consists of three successful components: WFRFT, PCA, and SVM (or its two variants, i.e., GEPSVM and TSVM). The implementation of this proposed system contains two folds: offline learning to train the classifier and online prediction to predict new instances. Figure 3 depicts the flowchart and Table I gives its

Table I. Pseudocode of the proposed method.

Offline learning
Step A. *Feature extraction*: Users performed WFRFT on all ground-truth images. For a given image, 25 different WFRFT operations were performed with α_x and α_y increasing from 0.6 to 1, with increase of 0.1, respectively.
Step B. *Feature reduction*: The 25 WFRFT results of each image were combined into a vector, and then PCA was performed on the WFRFT results of all images. The PC coefficients were recorded. The number of PCs was set as to cover 95% variances.
Step C. *Training*: Selected PCs together with their class labels were submitted to train the weights and biases of SVM or its two variants (GEPSVM and TSVM).
Step D. *Evaluation*: Record the classification performance based on a 5 × 5-fold cross-validation.
Online prediction
Step A. *Feature extraction*: The new brain image is submitted to this system, and 25 WFRFT results with the same predefined α_x and α_y were obtained.
Step B. *Feature reduction*: The 25 WFRFT results were multiplied with PC coefficients, and the reduced features were obtained.
Step C. *Prediction*: Users input the reduced features obtained from the query image to the trained SVM, in order to get the output of whether pathological or healthy.

Table II. WFRFT of a normal brain.

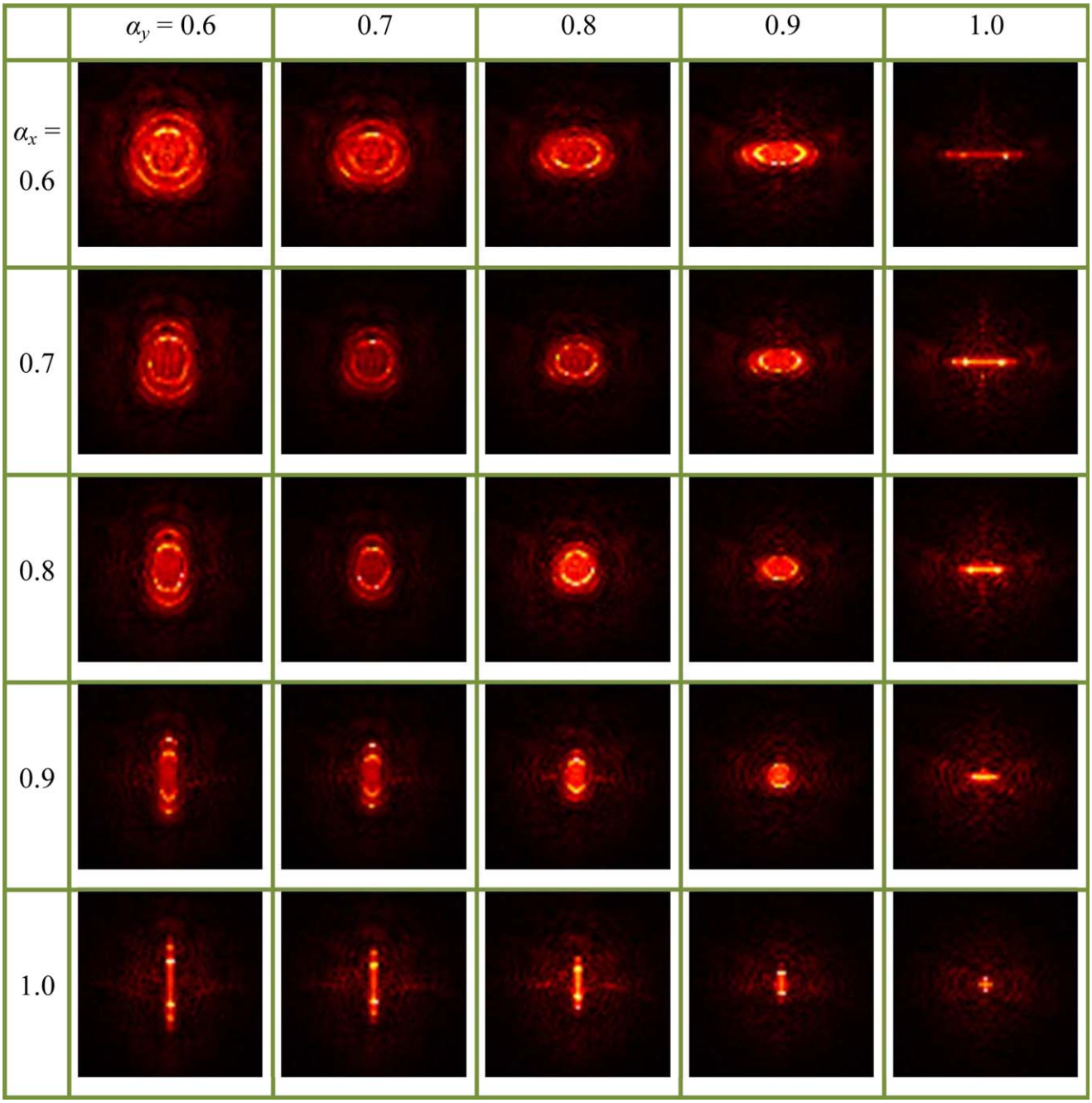

All images are log-enhanced and added with "hot" colormap for better view.

pseudocode. Note that offline learning and online prediction of PCA are different (Zhang et al., 2015).

3. EXPERIMENTS, RESULTS, AND DISCUSSIONS

The algorithm was developed in-house based on the signal processing toolbox of 64-bit Matlab 2014a (The Mathworks, Natick, MA). The simulation experiments were implemented on the platform of P4 IBM with 3.2 GHz processor, and 8 GB random access memory, running under Windows 7 operating system. The code of SVM can be performed by two simple commands: "svmtrain" and "svmclassify."

A. Feature Extraction. The different WFRFT results of a healthy MR brain are shown in Table II. Here we set both α_x and α_y to vary from 0.6 to 1 with equal increase of 0.1, respectively. When the angles increase to 1, the FRFT becomes similar to a conventional FT. In contrary, when the angles decrease to 0, the FRFT result is similar to original brain image. This is the reason why we choose the range of angles in between 0.6 and 1.

Some references proposed optical angle estimation (OAE) method to select the optimal angle of FRFT to transform a particular image to the optimal FRFT domain (Elgamel and Soraghan, 2011).

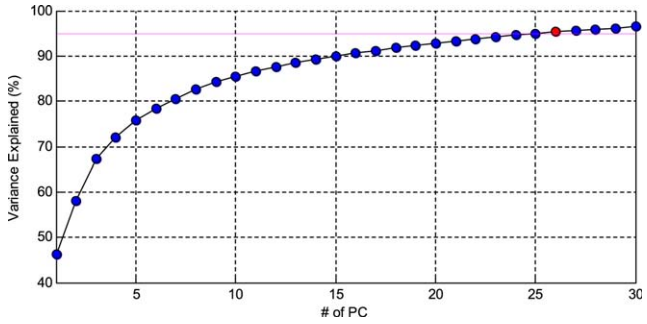

Figure 4. Select 26 PCs by the criterion of 95% variance. [Color figure can be viewed in the online issue, which is available at wileyonlinelibrary.com.]

Nevertheless, we believe that OAE method is not suitable for this study. The reason is that each angle corresponds to a totally different spectrum, and each spectrum contains its own information. Hence, our method (to provide a range for rotational angles and use PCA to reduce the features of spectrums) is better than the OAE method.

B. Feature Reduction. For each image, there are $25 \times 256 \times 256 = 1{,}638{,}400$ features. The data were centered to zero-mean before implementing PCA. The result is shown in Figure 4. Here x-axis denotes the number of PCs, and the y-axis the percentage of the total variance explained by each PC. The threshold lines were assigned with a value of 95%. Figure 4 shows that only 26 features can cover more than 95% of total variances.

C. Algorithm Comparison. The reduced features were fed into the SVM. We compared the three proposed "WFRFT + PCA + SVM," "WFRFT + PCA + GEPSVM," and "WFRFT + PCA + TSVM" methods with eight state-of-the-art methods: "DWT + PCA + BP-NN" (Zhang et al., 2013), "DWT + PCA + RBF-NN" (Zhang et al., 2013), "DWT + PCA + PSO-KSVM" (Zhang et al., 2013), "WE + PSO-KSVM" (Yang et al., 2015), "WE + BBO-KSVM" (Yang et al., 2015), "DWT + PCA + GA-KSVM" (Wang et al., 2015a), "WE + BPNN" (Choudhary et al., 2009), and "WE + KSVM" (Mookiah et al., 2012). The results are shown in Table III.

Results in Table III showed that the proposed "WFRFT + PCA + SVM" correctly matched 441 cases with sensitivity of 98.35%, specificity of 92.00%, precision of 99.52%, and accuracy of 98.00%. The proposed "WFRFT + PCA + GEPSVM" correctly matched 446 cases with sensitivity of 99.53%, specificity of 92.00%, precision of 99.53%, and accuracy of 99.11%. The proposed "WFRFT + PCA + TSVM" correctly matched 445 cases with sensitivity of 99.29%, specificity of 92.00%, precision of 99.53%, and accuracy of 98.89%.

Comparing with other algorithms on the basis of accuracy, we found that the three proposed methods achieved accuracy larger than 98.00, which outperforms all their competitors. The best among the state-of-the-art algorithms is "DWT + PCA + PSO-KSVM" (Zhang et al., 2013) and "WE + BBO-KSVM" (Yang et al., 2015) with accuracies of 97.78%, which are even less than the worst of our proposed methods (98.00% for WFRFT + PCA + SVM). Therefore, the proposed methods perform quite well. They indicate the effectiveness of WFRFT.

From Table III, it is difficult to state that GEPSVM is better than TSVM, because their results are closely similar to each other.

Table III. Classification comparison.

	Success Cases	Sensitivity (%)	Specificity (%)	Precision (%)	Accuracy (%)
Existing methods					
DWT + PCA + BP-NN (Zhang et al., 2013)	388	88.0	56.00	97.14	86.22
DWT + PCA + RBF-NN (Zhang et al., 2013)	411	92.47	72.00	98.25	91.33
DWT + PCA + PSO-KSVM (Zhang et al., 2013)	440	98.12	**92.00**	99.52	97.78
WE + PSO-KSVM (Yang et al., 2015)	437	97.65	88.00	99.28	97.11
WE + BBO-KSVM (Yang et al., 2015)	440	98.12	**92.00**	99.52	97.78
DWT + PCA + GA-KSVM (Wang et al., 2015a)	439	97.88	**92.00**	99.52	97.56
WE + BP-NN (Choudhary et al., 2009)	390	88.47	56.00	97.16	86.67
WE + KSVM (Mookiah et al., 2012)	413	93.18	68.00	98.02	91.78
Proposed methods					
WFRFT + PCA + SVM	441	98.35	**92.00**	99.52	98.00
WFRFT + PCA + GEPSVM	446	**99.53**	**92.00**	**99.53**	**99.11**
WFRFT + PCA + TSVM	445	99.29	**92.00**	**99.53**	98.89

Bold denotes the best.

DWT, discrete wavelet transform; PCA, principal component analysis; BP, back propagation; NN, neural network; RBF, radial basis function; KSVM, kernel support-vector machine; WE, wavelet-energy; GA, genetic algorithm; PSO, particle swarm optimization; BBO, biogeography-based optimization.

Table IV. Five-run results of WFRFT + PCA + GEPSVM.

	Fold 1	Fold 2	Fold 3	Fold 4	Fold 5	Sum
Run 1	18 (100.00%)	18 (100.00%)	18 (100.00%)	18 (100.00%)	18 (100.00%)	90 (100.00%)
Run 2	18 (100.00%)	17 (94.44%)	18 (100.00%)	18 (100.00%)	18 (100.00%)	89 (98.89%)
Run 3	18 (100.00%)	18 (100.00%)	18 (100.00%)	17 (94.44%)	18 (100.00%)	89 (98.89%)
Run 4	18 (100.00%)	18 (100.00%)	18 (100.00%)	18 (100.00%)	18 (100.00%)	90 (100.00%)
Run 5	17 (94.44%)	18 (100.00%)	18 (100.00%)	17 (94.44%)	18 (100.00%)	88 (97.78%)
Sum						446 (99.11%)

Table V. Time analysis.

	GEPSVM	TSVM
Offline training (s)	0.2495	0.0628
Online prediction (s)	0.0020	0.0021

Nevertheless, it is certain that GEPSVM and TSVM perform better than original SVM. This is due to the nonparallelism of the two hyperplanes of GEPSVM and TSVM. The nonparallel concept guarantees a flexibility to generate a more complicated hyperplane to separate the two classes.

Finally, all the images in the dataset are obtained from realistic people, so our methods may be used in practical in the near future.

D. Results on Each Run. To illustrate how to get the aforementioned results, we take "WFRFT + PCA + GEPSVM" as example and show in Table IV its result over each run and each fold.

E. Time Analysis. In the final experiment, we compared the computation time by GEPSVM and TSVM in both offline training and online prediction phases. The results are listed in Table V with unit of second.

The results in Table V show that GEPSVM and TSVM cost 0.2495 s and 0.0628 s, respectively, for offline training. The computation time of GEPSVM is more or less four times of that of TSVM. For online prediction, the GEPSVM and TSVM cost about the same time (0.0020s for GEPSVM and 0.0021s for TSVM).

4. CONCLUSIONS

In this article, we proposed three novel approaches for MR brain image classification: "WFRFT + PCA + SVM," "WFRFT + PCA + GEPSVM," and "WFRFT + PCA + TSVM." The results showed that the proposed methods yield better results than eight existing methods. This proposed classification system may further be used for classification of MR brain image with different pathological condition, types, and disease status.

The contributions of this article lie in following points: (i) We investigated the potential use of WFRFT in MR image classification and proved that WFRFT is effective; (2) The proposed system "WFRFT + PCA + GEPSVM" (or TSVM) is superior to the proposed "WFRFT + PCA + SVM" and eight state-of-the-art methods.

Future work should focus on the following points: (i) We will consider to use other imaging modalities, like ultrasound (Lee et al., 2014), MR spectroscopic imaging (Dong et al., 2014), computed tomography (Chen et al., 2008, 2009), and diffusion-tensor imaging (Huo et al., 2011); (ii) Other feature extraction methods will be tested, such as fractional wavelet, binary PSO (Zhang et al., 2014), and dual tree complex wavelet transform. (iii) Advanced classification methods will be included, such as RBFNN, fuzzy SVM (Wang et al., 2015b), and deep leaning. (iv) We will try to apply our method to remote-sensing, image reconstruction (Lee et al., 2012), and other related fields. (v) We will try other fast implementation approaches of FRFT. (vi) Obsessive-compulsive disorder (Marsh et al., 2015) will be added into our dataset. (vii) The proposed method may be applied to other animals such as rats (Lee et al., 2009).

ACKNOWLEDGMENT

The authors have no conflicts of interest to disclose with regard to the subject matter of this article.

REFERENCES

P.K. Ajmera and R.S. Holambe, Fractional Fourier transform based features for speaker recognition using support vector machine, Comput Electr Eng 39 (2013), 550–557.

B. Bhaduri, C.J. Tay, C. Quan, and C.J.R. Sheppard, Motion detection using extended fractional Fourier transform and digital speckle photography, Opt Express 18 (2010), 11396–11405.

N.D. Cagatay and M. Datcu, FrFT-based scene classification of phase-gradient InSAR images and effective baseline dependence, IEEE Geosci Remote Sens Lett 12 (2015), 1131–1135.

S. Chaplot, L.M. Patnaik, and N.R. Jagannathan, Classification of magnetic resonance brain images using wavelets as input to support vector machine and neural network, Biomed Signal Process Control 1 (2006), 86–92.

Y. Chen, D.Z. Gao, C. Nie, L.M. Luo, W.F. Chen, X.D. Yin, and Y.Z. Lin, Bayesian statistical reconstruction for low-dose X-ray computed tomography using an adaptive-weighting nonlocal prior, Comput Med Imaging Graph 33 (2009), 495–500.

Y. Chen, J.H. Ma, Q.J. Feng, L.M. Luo, P.C. Shi, and W.F. Chen, Nonlocal prior Bayesian tomographic reconstruction, J Math Imaging Vision 30 (2008), 133–146.

R. Choudhary, S. Mahesh, J. Paliwal, and D.S. Jayas, Identification of wheat classes using wavelet features from near infrared hyperspectral images of bulk samples, Biosyst Eng 102 (2009), 115–127.

S.K. Damarla and M. Kundu, Numerical solution of multi-order fractional differential equations using generalized triangular function operational matrices, Appl Math Comput 263 (2015), 189–203.

S. Damodharan and D. Raghavan, Combining tissue segmentation and neural network for brain tumor detection, Int Arab J Inf Technol 12 (2015), 42–52.

S. Das, M. Chowdhury, and M.K. Kundu, Brain MR image classification using multiscale geometric analysis of Ripplet, Prog Electromagn Res 137 (2013), 1–17.

Z. Dong, L. Wu, S. Wang, and Y. Zhang, A hybrid method for MRI brain image classification, Expert Syst Appl 38 (2011), 10049–10053.

Z. Dong, Y. Zhang, F. Liu, Y. Duan, A. Kangarlu, and B.S. Peterson, Improving the spectral resolution and spectral fitting of 1H MRSI data from human calf muscle by the SPREAD technique, NMR Biomed 27 (2014), 1325–1332.

E.S.A. El-Dahshan, T. Hosny, and A.B.M. Salem, Hybrid intelligent techniques for MRI brain images classification, Digital Signal Process 20 (2010), 433–441.

E.S.A. El-Dahshan, H.M. Mohsen, K. Revett, and A.B.M. Salem, Computer-aided diagnosis of human brain tumor through MRI: A survey and a new algorithm, Expert Syst Appl 41 (2014), 5526–5545.

S.A. Elgamel and J. Soraghan, Enhanced monopulse tracking radar using optimum fractional Fourier transform, IET Radar Sonar Nav 5 (2011), 74–82.

L. Fang, L. Wu, and Y. Zhang, A novel demodulation system based on continuous wavelet transform, Math Probl Eng 2015 (2015), 9.

P. Georgiadis, D. Cavouras, I. Kalatzis, A. Daskalakis, G.C. Kagadis, K. Sifaki, M. Malamas, G. Nikiforidis, and E. Solomou, Improving brain tumor characterization on MRI by probabilistic neural networks and non-linear transformation of textural features, Comput Methods Programs Biomed 89 (2008), 24–32.

S. Goh, Z. Dong, Y. Zhang, S. DiMauro, and B.S. Peterson, Mitochondrial dysfunction as a neurobiological subtype of autism spectrum disorder: Evidence from brain imaging, JAMA Psychiatry 71 (2014), 665–671.

Z. Guang-Shuai, W. Qiong, F. Chunmei, L. Elizabeth, J. Genlin, W. Shuihua, Z. Yudong, and Y. Jie, "Automated classification of brain MR images using wavelet-energy and support vector machines," In Proceedings of the 2015 international conference on mechatronics, electronic, industrial

and control engineering, C. Liu, G. Chang, and Z. Luo (Editors), Atlantis Press, Mountain View, CA, 2015, pp. 683–686.

R. Harikumar and B.V. Kumar, Performance analysis of neural networks for classification of medical images with wavelets as a feature extractor, Int J Imaging Syst Technol 25 (2015), 33–40.

Y. Huo, Y. Zhang, S. Wang, and L. Wu, Diffusion tensor image registration based on demon-affine method and FSGA-BFGS algorithm, J Convergence Inf Technol 6 (2011), 108–115.

Jayadeva, R. Khemchandani, and S. Chandra, Twin support vector machines for pattern classification, IEEE TPAMI 29 (2007), 905–910.

R. Khemchandani, A. Karpatne, and S. Chandra, Generalized eigenvalue proximal support vector regressor, Expert Syst Appl 38 (2011), 13136–13142.

M. Kuroda, Y. Mori, M. Iizuka, and M. Sakakihara, Acceleration of the alternating least squares algorithm for principal components analysis, Comput Stat Data Anal 55 (2011), 143–153.

W. Lee, C.Y. Bae, S. Kwon, J. Son, J. Kim, Y. Jeong, S.S. Yoo, and J.K. Park, Cellular hydrogel biopaper for patterned 3D cell culture and modular tissue reconstruction, Adv Healthcare Mater 1 (2012), 635–639.

W. Lee, S.D. Lee, M.Y. Park, J.C. Yang, and S.S. Yoo, Evaluation of polyvinyl alcohol cryogel as an acoustic coupling medium for low-intensity transcranial focused ultrasound, Int J Imaging Syst Technol 24 (2014), 332–338.

W. Lee, J. Pinckney, V. Lee, J.H. Lee, K. Fischer, S. Polio, J.K. Park, and S.S. Yoo, Three-dimensional bioprinting of rat embryonic neural cells, Neuroreport 20 (2009), 798–803.

O.L. Mangasarian and E.W. Wild, Multisurface proximal support vector machine classification via generalized eigenvalues, IEEE TPAMI 28 (2006), 69–74.

R. Marsh, G.Z. Tau, Z.S. Wang, Y. Huo, G. Liu, X.J. Hao, M.G. Packard, B.S. Peterson, and H.B. Simpson, Reward-based spatial learning in unmedicated adults with obsessive-compulsive disorder, Am J Psychiatry 172 (2015), 383–392.

S. Mehrkanoon, X.L. Huang, and J.A.K. Suykens, Non-parallel support vector classifiers with different loss functions, Neurocomputing 143 (2014), 294–301.

M.R.K. Mookiah, U.R. Acharya, C.M. Lim, A. Petznick, and J.S. Suri, Data mining technique for automated diagnosis of glaucoma using higher order spectra and wavelet energy features, Knowledge-Based Syst 33 (2012), 73–82.

C.R. Munteanu, C. Fernandez-Lozano, V.M. Abad, S.P. Fernandez, J. Alvarez-Linera, J.A. Hernandez-Tamames, and A. Pazos, Classification of mild cognitive impairment and Alzheimer's disease with machine-learning techniques using H-1 magnetic resonance spectroscopy data, Expert Syst Appl 42 (2015), 6205–6214.

J.A. Nasiri, N.M. Charkari, and K. Mozafari, Energy-based model of least squares twin support vector machines for human action recognition, Signal Process 104 (2014), 248–257.

M. Nazir, F. Wahid, and S.A. Khan, A simple and intelligent approach for brain MRI classification, J Intell Fuzzy Syst 28 (2015), 1127–1135.

H.M. Ozaktas, O. Arikan, M.A. Kutay, and G. Bozdagt, Digital computation of the fractional Fourier transform, IEEE Trans Signal Process 44 (1996), 2141–2150.

A. Padma and R. Sukanesh, Segmentation and classification of brain CT images using combined wavelet statistical texture features, Arab J Sci Eng 39 (2014), 767–776.

A.P. Punnen, P. Sripratak, and D. Karapetyan, The bipartite unconstrained 0-1 quadratic programming problem: Polynomially solvable cases, Discrete Appl Math 193 (2015), 1–10.

R. Ramasamy, P. Anandhakumar, Brain tissue classification of MR images using fast Fourier transform based expectation-maximization Gaussian mixture model, Adv Comput Inf Technol, 198 (2011), 387–398.

V. Rodriguez-Galiano, M. Sanchez-Castillo, M. Chica-Olmo, and M. Chica-Rivas, Machine learning predictive models for mineral prospectivity: An evaluation of neural networks, random forest, regression trees and support vector machines, Ore Geol Rev 71 (2015), 804–818.

B. Santhanam and J.H. McClellan, The discrete rotational Fourier transform, IEEE Trans Signal Process 44 (1996), 994–998.

M. Saritha, K. Paul Joseph, and A.T. Mathew, Classification of MRI brain images using combined wavelet entropy based spider web plots and probabilistic neural network, Pattern Recogn Lett 34 (2013), 2151–2156.

A. Savio and M. Grana, Local activity features for computer aided diagnosis of schizophrenia on resting-state fMRI, Neurocomputing 164 (2015), 154–161.

J. Seok and K. Bae, Target classification using features based on fractional Fourier transform, IEICE Trans Inf Syst E97D (2014), 2518–2521.

Y.H. Shao, W.J. Chen, J.J. Zhang, Z. Wang, and N.Y. Deng, An efficient weighted Lagrangian twin support vector machine for imbalanced data classification, Pattern Recogn 47 (2014), 3158–3167.

Y.H. Shao, N.Y. Deng, W.J. Chen, and Z. Wang, Improved generalized eigenvalue proximal support vector machine, IEEE Signal Process Lett 20 (2013), 213–216.

C.C. Shih, Fractionalization of Fourier transform, Opt Commun 118 (1995), 495–498.

F. Thorsen, B. Fite, L.M. Mahakian, J.W. Seo, S.P. Qin, V. Harrison, S. Johnson, E. Ingham, C. Caskey, T. Sundstrom, T.J. Meade, P.N. Harter, K.O. Skaftnesmo, and K.W. Ferrara, Multimodal imaging enables early detection and characterization of changes in tumor permeability of brain metastases, J Control Release 172 (2013), 812–822.

S. Wang, Z. Dong, G. Ji, and Y. Zhang, Classification of Alzheimer disease based on structural magnetic resonance imaging by kernel support vector machine decision tree. Prog Electromagn Res 144 (2014), 171–184.

S. Wang, G. Ji, P. Phillips, Z. Dong, "Application of genetic algorithm and kernel support vector machine to pathological brain detection in MRI scanning," In The 2nd national conference on information technology and computer science (CITCS2015), A. Hu (Editor), DEStech Publications, Lancaster, 2015a, pp. 450–456.

S. Wang and L. Wu, A novel method for magnetic resonance brain image classification based on adaptive chaotic PSO, Prog Electromagn Res 109 (2010), 325–343.

S. Wang, X. Yang, Y. Zhang, P. Phillips, J. Yang, and T.F. Yuan, Identification of green, oolong and black teas in China via wavelet packet entropy and fuzzy support vector machine, Entropy 17 (2015b), 6663–6682.

S. Wang, Y. Zhang, Z. Dong, S. Du, G. Ji, J. Yan, J. Yang, Q. Wang, C. Feng, and P. Phillips, Feed-forward neural network optimized by hybridization of PSO and ABC for abnormal brain detection, Int J Imaging Syst Technol 25 (2015c), 153–164.

S. Wang, Y. Zhang, G. Ji, J. Yang, J. Wu, and L. Wei, Fruit classification by wavelet-entropy and feedforward neural network trained by fitness-scaled chaotic ABC and biogeography-based optimization, Entropy 17 (2015d), 5711–5728.

A. Wibmer, H. Hricak, T. Gondo, K. Matsumoto, H. Veeraraghavan, D. Fehr, J.T. Zheng, D. Goldman, C. Moskowitz, S.W. Fine, V.E. Reuter, J. Eastham, E. Sala, and H.A. Vargas, Haralick texture analysis of prostate MRI: Utility for differentiating non-cancerous prostate from prostate cancer and differentiating prostate cancers with different Gleason scores, Eur Radiol 25 (2015), 2840–2850.

L. Wu and S. Wang, Magnetic resonance brain image classification by an improved artificial bee colony algorithm, Prog Electromagn Res 116 (2011), 65–79.

L. Wu and Y. Zhang, Classification of fruits using computer vision and a multiclass support vector machine, Sensors 12 (2012), 12489–12505.

Z.J. Xu, Z.Q. Qi, and J.Q. Zhang, Learning with positive and unlabeled examples using biased twin support vector machine, Neural Comput Appl 25 (2014), 1303–1311.

G. Yang, Y. Zhang, J. Yang, G. Ji, Z. Dong, S. Wang, C. Feng, and Q. Wang, Automated classification of brain images using wavelet-energy and biogeography-based optimization, Multimedia Tools Appl (2015), 1–17, doi: 10.1007/s11042-015-2649-7 [Epub ahead of print].

D. Yu, H. Shui, L. Gen, and C. Zheng. Exponential wavelet iterative shrinkage thresholding algorithm with random shift for compressed sensing magnetic resonance imaging, IEEJ Trans Electr Electr Eng 10 (2015), 116–117.

Y. Zhang, Z. Dong, G. Ji, and S. Wang, Effect of spider-web-plot in MR brain image classification, Pattern Recogn Lett 62 (2015a), 14–16.

Y. Zhang, Z. Dong, A. Liu, S. Wang, G. Ji, Z. Zhang, and J. Yang, Magnetic resonance brain image classification via stationary wavelet transform and generalized eigenvalue proximal support vector machine, J Med Imaging Health Informatics 5 (2015b), 1395–1403.

Y. Zhang, Z. Dong, P. Phillips, S. Wang, G. Ji, and J. Yang, Exponential wavelet iterative shrinkage thresholding algorithm for compressed sensing magnetic resonance imaging, Inf Sci 322 (2015c), 115–132.

Y. Zhang, Z. Dong, P. Phillips, S. Wang, G. Ji, J. Yang, and T.F. Yuan, Detection of subjects and brain regions related to Alzheimer's disease using 3D MRI scans based on eigenbrain and machine learning, Front Comput Neurosci 66 (2015d), 1–15.

Y. Zhang, Z. Dong, S. Wang, G. Ji, and J. Yang, Preclinical diagnosis of magnetic resonance (MR) brain images via discrete wavelet packet transform with Tsallis entropy and generalized eigenvalue proximal support vector machine (GEPSVM), Entropy 17 (2015e), 1795–1813.

Y. Zhang and S. Wang, Detection of Alzheimer's disease by displacement field and machine learning, PeerJ 3 (2015), e1251.

Y. Zhang, S. Wang, Z. Dong, P. Phillips, G. Ji, and J. Yang, Pathological brain detection in magnetic resonance imaging scanning by wavelet entropy and hybridization of biogeography-based optimization and particle swarm optimization, Prog Electromagn Res 152 (2015f), 41–58.

Y. Zhang, S. Wang, G. Ji, and Z. Dong, An MR brain images classifier system via particle swarm optimization and kernel support vector machine, Sci World J 2013 (2013), 9.

Y. Zhang, S. Wang, G. Ji, and J. Yan, A note on Das's PCA in online phases, Prog Electromagn Res Lett 51 (2015g), 117–118.

Y. Zhang, S. Wang, P. Phillips, and G. Ji, Binary PSO with mutation operator for feature selection using decision tree applied to spam detection, Knowledge-Based Syst 64 (2014), 22–31.

Y. Zhang, S. Wang, P. Sun, and P. Phillips, Pathological brain detection based on wavelet entropy and Hu moment invariants, Biomed Mater Eng 26 (2015h), 1283–1290.

Y. Zhang and L. Wu, An MR brain images classifier via principal component analysis and kernel support vector machine, Prog Electromagn Res 130 (2012), 369–388.

X. Zhou, S. Wang, W. Xu, G. Ji, P. Phillips, P. Sun, Y. Zhang, "Detection of pathological brain in MRI scanning based on wavelet-entropy and Naive Bayes classifier," In Bioinformatics and biomedical engineering, F. Ortuño and I. Rojas (Editors), Springer International Publishing, Granada, Spain, 2015, pp. 201–209.